

# Confinement Related Phenomena in MoS<sub>2</sub> Tubular Structures Grown from Vapour Phase

Maja Remskar,<sup>[a, b]</sup> Andreas K. Hüttel,<sup>[c]</sup> Tatiana V. Shubina,<sup>[d]</sup> Alan Seabaugh,<sup>[e]</sup> Sara Fathipour,<sup>[e]</sup> Robert Lawrowski,<sup>[f]</sup> and Rupert Schreiner<sup>[f]</sup>

**Abstract:** We review recently discovered phenomena observed in the MoS<sub>2</sub> tubular structures, which were synthesized by a lasting chemical transport reaction nearly at chemical equilibrium. Such MoS<sub>2</sub> nanotubes are distinguished by low density of structural defects, thin walls and a high aspect ratio, which intrinsically provide a confined, edge-free geometry. Quantum confinement with single

electron conductance was recorded and a bright exciton photoluminescence with appearance of whispering gallery modes was observed. In addition, the field-effect transistors and field emitters based on single MoS<sub>2</sub> nanotubes were demonstrated. These discoveries revitalize research of MoS<sub>2</sub> curved structures grown from vapour phase, which were reported several decades ago.

## 1. Introduction

MoS<sub>2</sub> belongs to earth-abundant layered transition metal dichalcogenide (TMDC) compounds, and has attracted a lot of attention in last decade due to its semiconducting properties and indirect-to-direct band gap transition in the monolayer limit. It is stable in various allotropes.<sup>[1]</sup> Bulk-MoS<sub>2</sub> (synthetic and as mineral molybdenite) is applicable as low-friction additive due to weak van der Waals interaction between the layers and as catalysts for desulphurization of petroleum and hydrogenation of organic compounds. The MoS<sub>2</sub> is stable also as thin curved plates, rolls, nanorods, micro- and nanotubes, ribbons and fullerene-like nano-onions, and in atomically-thin two-dimensional (2D) structure.<sup>[2]</sup> Different procedures for their synthesis are collected in recent review by U. Krishan et al.,<sup>[3]</sup> while electrical and optical properties were reviewed by H. S. Nalwa<sup>4</sup> in 2020. The main building block is a S–Mo–S molecular layer with hexagonal arrangement of side S and inner Mo atomic planes. Stacking of these triple layers differs in various polytypes and determines their stability at different temperature and pressure conditions as well as it affects their electronic properties. In contrary with strong ionic-covalent interactions among intra-plane atoms, relatively weak interactions between these layers enables easy mutual gliding, which is important for lubrication properties and also for preparing ultrathin crystals of MoS<sub>2</sub> by cleavage technique. The most stable structure in a flat geometry is the hexagonal (2H) polytype with two molecular layers in the unit cell and semiconducting properties with an indirect band gap of ~1.3 eV.<sup>[5]</sup> Another stable structure (found also in minor quantities in mineral molybdenite) is a rhombohedral (3R) polytype with three molecular layers in the unit cell and the space group R3m, which transforms to 2H under heating. 3R-MoS<sub>2</sub> exhibits nonlinear optical properties due to broken inversion symmetry in thin films with odd number of layers. Second harmonic generation efficiency by two orders of magnitude larger than that of 2H bulk MoS<sub>2</sub> was reported<sup>[6]</sup>

and applications for valleytronics were proposed.<sup>[7]</sup> While in both 2H and 3R polytypes, Mo atoms are trigonally prismatic coordinated with S atoms, they are octahedrally coordinated in the metastable 1T-MoS<sub>2</sub> allotrope, which undergoes an irreversible phase transition to a disordered 2H-MoS<sub>2</sub> polymorph at 95 °C.<sup>[8]</sup> With decreasing thickness of MoS<sub>2</sub> crystals, a progressive confinement-induced shift in the indirect gap from the bulk value to over 1.90 eV was observed<sup>[9]</sup> with value for the monolayer MoS<sub>2</sub> bandgap from 2.8 eV to 1.9 eV being dependent on dielectric environment.<sup>[10]</sup> The absence of chemical bonds between the molecular layers enables formation of curved structures, where the curvature of the lattice causes a slight mutual detachment of the molecular layers.<sup>[11]</sup> Self-terminated layers in forms of tubes and onions are

[a] *M. Remskar*  
Jozef Stefan Institute, Jamova 39, 1000 Ljubljana, Slovenia

[b] *M. Remskar*  
Faculty of Mathematics and Physics, University of Ljubljana, Jadranska Cesta 19, 1000 Ljubljana, Slovenia

[c] *A. K. Hüttel*  
Institute for Experimental and Applied Physics, University of Regensburg, 93040 Regensburg, Germany

[d] *T. V. Shubina*  
Ioffe Institute, 26 Politekhnicheskaya, St. Petersburg 194021, Russia

[e] *A. Seabaugh, S. Fathipour*  
Department of Electrical Engineering, University of Notre Dame, Notre Dame, Indiana 46556, USA

[f] *R. Lawrowski, R. Schreiner*  
OTH Regensburg, Fakultät ANK, Seybothstr. 2, 93053 Regensburg, Germany

© 2021 The Authors. *Israel Journal of Chemistry* published by Wiley-VCH GmbH. This is an open access article under the terms of the Creative Commons Attribution Non-Commercial NoDerivs License, which permits use and distribution in any medium, provided the original work is properly cited, the use is non-commercial and no modifications or adaptations are made.

stabilized by the elimination of dangling bonds at the edges of molecular layers.

Here, we review MoS<sub>2</sub> curved structures prepared by chemical transport reaction grown from vapour phase. This method was overlooked in the review by U. Krishan et al.,<sup>[3]</sup>



Prof. Maja Remskar is a physicist, a senior scientist at Jozef Stefan Institute, Slovenia and professor at University in Ljubljana, Faculty for Mathematics and Physics, where she obtained PhD in 1994. She has discovered different shapes of nanomaterials, especially of transition metal compounds. Her bibliography contains 147 original scientific articles, which were cited more than 6000 times with h-index of 33. She is a co-inventor of 5 international patents in fields of nanotechnology and detection of nanoparticles in air. Her research interests are Mo- and W-based nanomaterials applicable in tribology, antimicrobial coatings, and catalysis.



Prof. Alan Seabaugh is a professor of electrical engineering at the University of Notre Dame and director of Notre Dame Nanoscience and Technology (NDnano). He received the Ph.D. degree in electrical engineering from the University of Virginia, Charlottesville, in 1985. He has authored or co-authored more than 300 papers and holds 24 U.S. patents. He received the Int. Symp. on Comp. Semicon. Quantum Devices Award in 2011 for seminal contributions and leadership in semiconductor devices and circuits based on quantum mechanical tunnelling. His research interests are nano-electronic devices and circuits, including the use of ferroelectric and ionic polymer dielectrics for memory, and steep transistors for low voltage computing and imaging.



Dr. Andreas K. Hüttel, DFG Heisenberg research fellow and research group leader at Univ. of Regensburg, specializes in low-temperature transport experiments on quantum materials and quantum devices. Recipient of the Walter Schottky Prize of the German Physical Society 2021, he obtained his Habilitation (venia legendi) in Physics at Regensburg in 2017 and his PhD at Ludwig-Maximilians-University Munich in 2005. With multiple publications in high-level journals such as Science, Nano Letters, Nature Commun., Phys. Rev. Lett, he has reached over 2000 citations and h-index of 18. His current research interests are MoS<sub>2</sub> transport spectroscopy and microwave optomechanics involving suspended carbon nanotubes.



Robert Lawrowski, MSc. received the M.Sc. degree in Applied Research in Engineering Science in 2014 from the OTH Regensburg (Germany). Since 2015 he is working in the Laboratory of Microsystems Technology at OTH Regensburg in the group of Prof. Rupert Schreiner as a Research Assistant. His PhD thesis in cooperation with the Technical University of Braunschweig and the OTH Regensburg will be completed in October 2021. Since 2021, Robert Lawrowski has been working in the research department of Osram Opto Semiconductors in Regensburg on the development of novel light-emitting diodes.



Prof. Tatiana V. Shubina, chief researcher at the Center for Physics of Nano-Heterostructures at the Ioffe Institute, has been engaged in solid state physics for over 30 years, specializing in optical spectroscopy, plasmonics, nanophotonics, and physics of nanostructures. Habilitation (Russian Doctor of Physical-Mathematical Sciences) was in 2009. She has published about 240 peer-reviewed papers, a monograph: "Plasmon Effects in Metal-Semiconductor Nanostructures," and a chapter on slow light. In total, more than 3000 citations of her works can be found, which corresponds to h-index 28 (index i10~90). Her current research interests are in the physics of 2D crystals and related nanostructures.



Prof. Rupert Schreiner received the Ph.D. degree from Stuttgart University, Stuttgart, Germany, in 2002. In 2001, he joined Infineon Technologies, Munich, Germany, to work on optoelectronic microsystems. Between 2004 and 2005 he was appointed as CTO of Parolink Technologies in Hsinchu Science Park (Taiwan). 2005 and 2006 he was project manager in the Technology Transfer of Infineon from Villach (Austria) to Kulim (Malaysia). Since 2006 he is Professor of Applied Physics at the Faculty of Microsystems Technology at the Ostbayerische Technische Hochschule (OTH) in Regensburg, Germany. His major research interests are microsystems, microsensors and optoelectronics.



Dr. Sara Fathipour received her PhD degree in 2017 from the University of Notre Dame, Notre Dame, IN, USA. She is currently a device engineer with Intel, Portland, OR, USA. Her research interests are emerging materials and devices for storage and computation, novel non-volatile memory technology and semiconductor device physics, fabrication and characterization.

despite the fact that it allows one to create various MoS<sub>2</sub> nanostructures with relatively small number of structural defects. Recently, interesting phenomena were observed in these tubular structures such as single electron conductance<sup>[12]</sup> and appearance of whispering gallery modes.<sup>[13]</sup> In addition, the designs of field-effect transistors<sup>[14]</sup> and field emitters<sup>[15]</sup> based on MoS<sub>2</sub> tubes were demonstrated. These recent discoveries revitalize research of MoS<sub>2</sub> curved structures grown from vapour phase several decades ago.

## 2. Some MoS<sub>2</sub> Curved Allotropes

The first MoS<sub>2</sub> nanotubes synthesized in R. Tenne's group in 1993 have been prepared by sulphurization of the MoOx-based precursor exposed to H<sub>2</sub>S atmosphere at a temperature above 800 °C.<sup>[16,17]</sup> A self-sacrificial growth mode was used, where outer shape of the crystals was determined by morphology of MoOx rods. The cylindrical geometry was caused by minimization of the free energy by self-termination of molecular layers growing in the sulphurization process, while hollow geometry was caused due to the difference in mass density of metal oxides and metal sulphides. In contrast to this precursor transformation process, curved MoS<sub>2</sub> of various morphologies can also grow directly from vapour phase

(Figure 1). The first MoS<sub>2</sub> tubes synthesized by chemical transport reaction were reported in 1996.<sup>[11]</sup> The synthesis took place in a two-zone furnace, using iodine as a transport agent. MoS<sub>2</sub> micro- and nanotubes were always grown together with thin and strongly undulated MoS<sub>2</sub> crystal flakes.<sup>[2]</sup> The tubes grow up to hundreds of micrometres in length with a wall thickness depending on the diameter, which ranges from around 20 nm up to above 10 μm. In tubes with diameter below a few hundred nm, wall thicknesses range between 25–30% of the tube diameter, while in micrometer diameter tubes, walls are relatively thin and independent on diameter, and reach a thickness of up to 100 nm. The nanotubes are hollow and open ended. They grow in a chiral mode with a similar angle of chirality,  $\alpha = 16^\circ \pm 0.5^\circ$ .<sup>[4]</sup>

Nucleation happens in wrinkles or at edges of thin MoS<sub>2</sub> flakes where the growth of the next basal MoS<sub>2</sub> plane cannot follow the bent substrate. The lost interaction with the substrate and simultaneous continuation of growth of such a mechanically unstable two-dimensional film are the proposed reasons for formation of scrolls, which is a thermally driven process. The scrolls can transform to tubes if one of the possible stacking orders (2H, 3R) is satisfied in the walls structure. Growth of a MoS<sub>2</sub> tube is very rigid. The diameter and wall thickness of a particular tube is extremely homogeneous over several hundred μm or even at mm range scale.

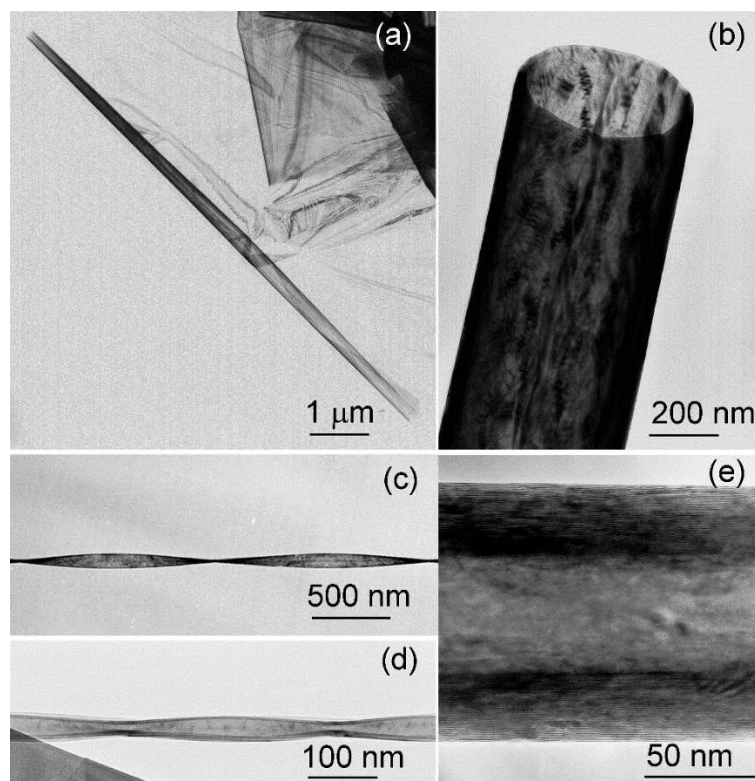


**Figure 1.** Some MoS<sub>2</sub> allotropes synthesized from the vapour phase in a temperature gradient: (a) a scroll of thin flake; (b) a nanotube with diameter of 520 nm; (c) a ribbon 88 nm wide; (d) a “breathing” nanotube; (e) a nanotube with diameter of 118 nm and wall thickness of 32 nm.

The MoS<sub>2</sub> tubes always grow on the top of thin MoS<sub>2</sub> flakes, i.e. in the second part of the growth process, when the flakes were already formed. The conditions for growth of tubes are of chemical (partial pressures) and physical (temperature, transport flow, shape of thin flakes as nucleation sites) origin. Because they grow on a very rough substrate of curved flakes, there is a high probability that the tubes meet a kind of obstacle during the longitudinal growth. If a tube comes to a physical contact with a platelet, a material from the flake is consumed for the growth of the tube leaving an empty hole in the flake. Such material translocation evidences energetically favourable growth of a tubular structure in comparison with flat geometry in this particular phase of growth process.<sup>[18]</sup> Another possible avoidance of an obstacle during the growth is a partial or complete collapse of cylindrical structure to a form of a ribbon.<sup>[19]</sup> Such collapsed tubes are usually twisted along their longitudinal length due to chiral growth mode of a pristine nanotube, which has been collapsed. The highly strained lattice of the walls at the ribbon edges is relaxed by the formation of undulations.<sup>[13]</sup> Ribbons are much softer against bending and are able to avoid growth obstacles. Therefore, they continue in longitudinal growth in a shape of a ribbon. The ribbons represent a new crystal phase of a solid matter and are still awaiting detailed studies and theoretical consideration. Besides the cylindrical shape of tubes and ribbon-like shape of collapsed tubes, some intermediate forms also exist, where a tube is more or less deformed from ideal cylindrical shape, but the walls are still separated along its diameter. The helicity due to chiral growth mode depends on diameter and wall thickness of such a “breathing” tube. Stabilization of these structures is caused by the interplay of curvature energy and the minimization of structural deformations by preserving of the stacking order among the adjacent molecular layers. The cross section of the breathing tubes is typically asymmetric with regard to its geometrical centre and resembles a pear-like shape, sometimes with an unequal number of molecular layers in semi-halves.

Polytypic variety is a characteristic also for MoS<sub>2</sub> in tubular shape and depends on a tube's diameter.<sup>[20]</sup> The 2H stacking sequence was found in nanotubes less than 200 nm in diameter, while in tubes with a diameter in the micron range, the lattice crystallized in the rhombohedral (3R) stacking order. Stabilization of this polytype, which is otherwise stable at elevated pressure above 4 GPa, is indirect evidence of the presence of strain built into the wall of the microtube. The intensity of the strain increases towards the tube axis, causing the contraction of interlayer distance and instability of the inner molecular layers at the place where the incorporated strain is relaxed with the creation of edge dislocations or stacking faults. In nanotubes with diameter below 200 nm, the strain is relaxed, stabilizing the hexagonal (2H) stacking sequence.

### 3. Physical Phenomena and Applicable Properties in Curved MoS<sub>2</sub> Structures

#### 3.1 Quantum Confinement in MoS<sub>2</sub> Nanotubes

Over the past decades carbon nanotubes have attracted immense scientific attention regarding low-temperature transport spectroscopy and single electron quantum phenomena.<sup>[21,22,23]</sup> Conversely, barely any experimental low-temperature transport work exists on one-dimensional MoS<sub>2</sub> nanostructures. Reaching quantum confinement in two-dimensional TMDC materials, under intense investigation worldwide, is a hard technical problem: while classical Coulomb blockade is routinely observed,<sup>[24,25]</sup> the large effective electron mass<sup>[26]</sup>  $m^* \sim 0.7 m_e$  places stringent limits on the confinement scales for single level transport. A long, low-defect density nanotube or nanoribbon intrinsically provides a restricted, edge-free geometry and thus potentially allows easier access to discrete quantum states.

From a theoretical point of view, multiple types of novel physics can be expected. MoS<sub>2</sub> nanotubes are semiconducting independent on chirality.<sup>[27]</sup> While planar MoS<sub>2</sub> is as monolayer a direct band gap and as multilayer an indirect band gap semiconductor,<sup>[28]</sup> single-wall MoS<sub>2</sub> nanotubes are expected to show a dependence on diameter and precise chirality.<sup>[29]</sup> Strong spin-orbit interaction in combination with a broken inversion symmetry leads to a spin-split band structure, both in the valence and (less so) in the conduction band. Planar MoS<sub>2</sub> exhibits intrinsic superconductivity with a “dome” of critical temperature as function of charge density,<sup>[30,31]</sup> similar to cuprate superconductors; the onset of superconductivity may be associated with a multi-valley Fermi surface.<sup>[32]</sup>

The fabrication of single MoS<sub>2</sub> nanotube devices<sup>[12]</sup> is derived from 2D material “scotch tape” techniques<sup>[33]</sup> similar to early carbon nanotube devices.<sup>[34]</sup> MoS<sub>2</sub> nanotubes are picked up from a growth substrate using an adhesive tape and deposited onto a Si++/SiO<sub>2</sub> wafer with marker patterns (Figure 2a). The deposited nanotubes are located via optical microscopy; contact electrodes are then designed and written using electron beam lithography.

A significant technical challenge is to obtain good electrical contact with the semiconductor, i.e. producing only negligible Schottky barriers at the metal-semiconductor interface. Metallic contacts on MoS<sub>2</sub> lead via a hybridization of the metal and semiconductor wavefunctions at the material interface to so-called metal-induced gap states. As a result, the Fermi level in MoS<sub>2</sub> is pinned near the conduction band edge,<sup>[35]</sup> suggesting the preference of contact metals with low work function. Indeed, with this approach, best results have been obtained by using titanium and scandium contacts.<sup>[36]</sup> The data of Figure 2 was obtained using Sc/Au contacts and a highly doped Si substrate as the back gate.

Figure 2c displays a transport spectrum of a MoS<sub>2</sub> nanotube device, with a zoom shown in Figure 2d. As a narrow, repetitive saw-tooth pattern clear Coulomb oscillations of the

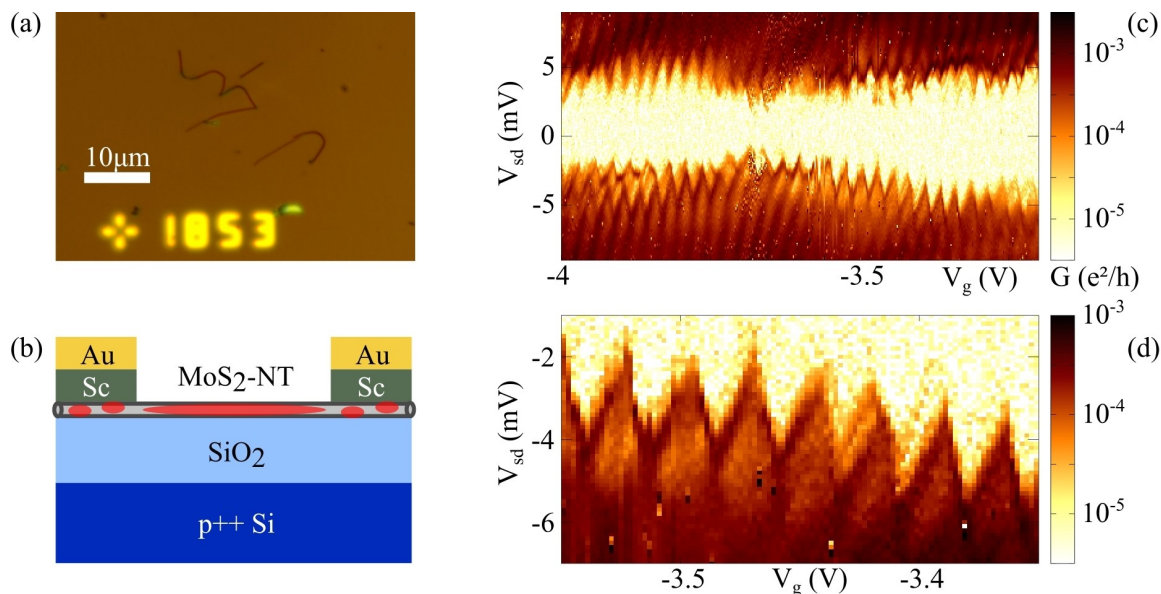


**Figure 2.** (adopted from Ref. 12): (a) Optical microscope image of MoS<sub>2</sub> nanotubes transferred onto a Si/SiO<sub>2</sub> wafer; (b) Schematic device, with Sc/Au contacts to the nanotube and the highly doped Si substrate as back gate. The red ellipses illustrate the formation of electronic traps below reactive metals, see the text; (c) Overview measurement of the differential conductance of a MoS<sub>2</sub> nanotube device at T = 300 mK; (d) Detail from (c).

conductance are visible. The total capacitance of the corresponding quantum dot can be estimated from the pattern and is consistent with a single electronic system occupying the entire nanotube between the contacts. The transport gap around zero bias indicates a voltage drop via trap states at the metallic contacts. Low work function metals are known to be reactive and to attack the MoS<sub>2</sub> crystal structure on surface deposition. In particular Ref. 37 demonstrates this via atomic scale imaging; the high Ti-S affinity leads there to the penetration of Ti and to structure degradation up to 5 planar MoS<sub>2</sub> layers deep. Such processes provide a likely explanation for the trap states and thus an intrinsic limitation of the low-work function metal approach.

Interestingly, the single electron tunnelling regions display traces of finite bias conductance resonances, marked in the zoom of Figure 2d. These may be related to discrete quantum excitations of the trapped electronic system; in the case of 1d confinement the level spacing becomes proportional to the number of charges on the quantum dot, as has already been observed in semiconductor nanowires.<sup>[12]</sup>

Future work will have to focus on improving the spectroscopic quality. As a specific outlook, the recent discovery<sup>[38]</sup> that the half-metal bismuth forms excellent Ohmic contacts to monolayer MoS<sub>2</sub> due to the suppression of metal-induced gap states provides a highly promising alternative approach.

### 3.2 MoS<sub>2</sub> Nanotubes as Optical Resonators

Bright exciton photoluminescence (PL) in the TMDC tubular structures prepared from vapour phase was discovered almost two decades after their first creation.<sup>[13,39]</sup> The micro-PL spectra of the individual MoS<sub>2</sub> tubes, shown in Figure 3, exhibit distinct resonances of A and B direct excitons over a wide temperature of 10–300 K. This observation contradicts the fact that many constituent monolayers in the tube walls suggest an electronic structure typical of a bulk material, which has an indirect band gap of about 1.3 eV<sup>[9]</sup> and should exhibit rather weak emission of indirect exciton transitions. Indirect exciton PL in the nanotubes arises at 70–100 K and increases in intensity with increasing temperature. This behavior reflects the competition between the two recombination channels through direct exciton transitions and phonon-assisted indirect ones.<sup>[40]</sup> The balance between them is mainly controlled by the oscillator strength of exciton resonances and the corresponding recombination rate, which is very high in the case of the direct transitions. In addition, the suppression of 1.3 eV emission at low temperature can indicate the optically forbidden dark state as the lowest in multilayered structures.<sup>[41]</sup>

The MoS<sub>2</sub> micro- and nanotubes, similarly to other tubular structures,<sup>[43]</sup> can confine the electromagnetic field inside their walls. In this case, two waves propagating in opposite directions form standing waves, called whispering gallery modes (WGMs). As a result, the tubes can act as an effective optical resonator – a microcavity, capable of supporting WGMs in the spectral ranges of both direct (1.8 eV) and indirect (1.3 eV) excitons (Figure 3a). It was found experimen-

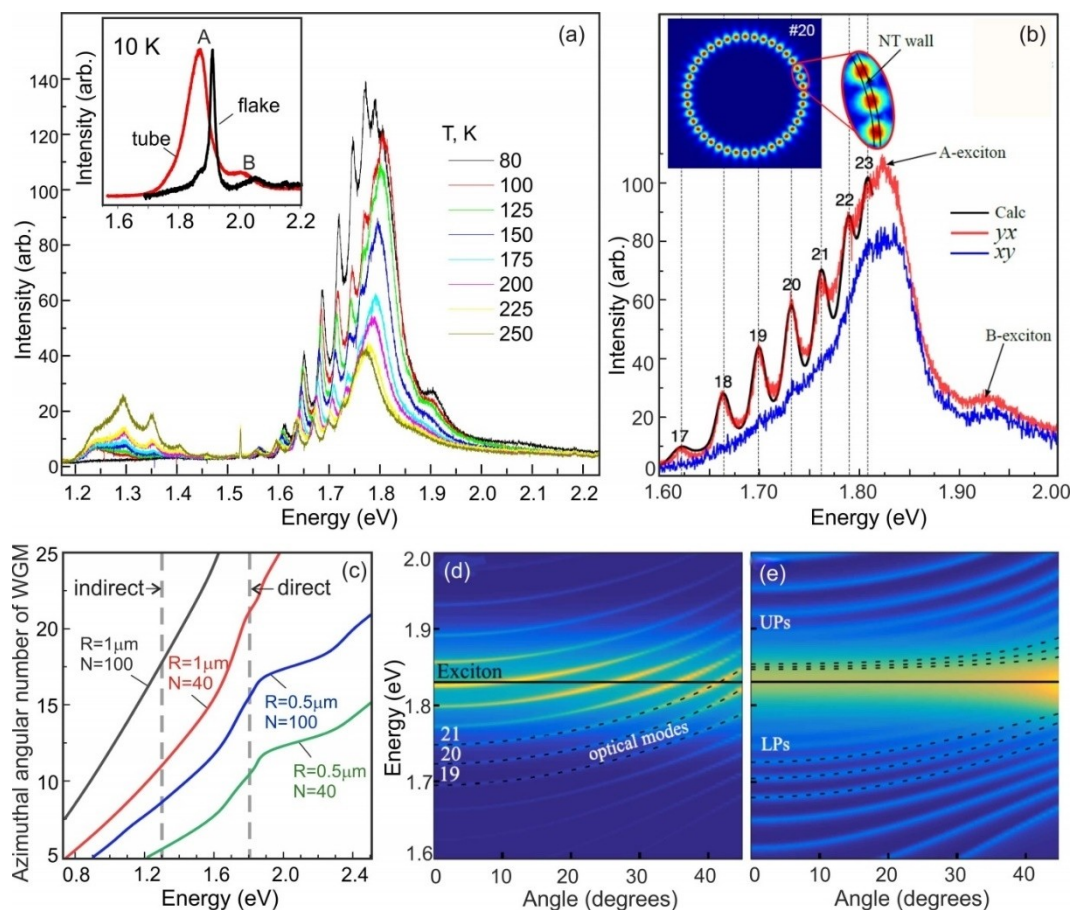


**Figure 3.** (a) Micro-PL spectra measured in a MoS<sub>2</sub> tube with a diameter of 2 μm in the range 10–250 K (adopted from Ref. 40). The inset shows the spectra measured at 10 K in a 400-nm nanotube and a flake grown in the same growth cycle. (b) Micro-PL spectra measured in different polarization configurations and the calculated PL spectrum, which reproduces sharp WGM peaks possessing different azimuthal angular numbers,  $m$ , marked in plot (adopted from Ref. 13). The inset shows the electric field distribution for the mode with  $m=20$  (the modeling is described in Ref. 13). (c) Dependencies of the mode angular numbers near direct and indirect excitons, calculated for different radii,  $R$ , and numbers of monolayers,  $N$ . (d, e) Emission spectra calculated for Rabi splitting of 2 meV (d) and 20 meV (e), as described in Ref. 42 (adopted from Ref. 43). The formation of upper (UPs) and lower (LPs) polaritons with increasing the Rabi splitting is shown in (e). The dispersion of optical modes and the energy of direct exciton are shown by dotted and solid lines.

tally, that the micro-PL spectra measured in individual nanotubes with a diameter of more than 500 nm are modulated by sharp WGM peaks, while these peaks are absent in tubes with a smaller diameter. This phenomenon reflects the fact that a certain number of wavelengths must fit along the tube diameter in order to form a WGM. Note that these modes were not observed in the flakes and ribbons which do not possess cylindrical geometry.

The WGM peaks are strongly polarized along the tube axis ( $yx$  and  $xx$  polarization configurations) that corresponds to TM-polarized optical modes (Figure 3b), while in two other configurations,  $xy$  and  $yy$ , the peaks are not pronounced.<sup>[13]</sup> The difference arises from the different azimuthal angular numbers,  $m$ , which are about twice higher for the TM modes (the higher the angular number, the more effective the enhancement provided by the optical mode). Figure 3c shows how this important parameter spectrally changes in tubes with different

radii and wall thicknesses. Low values of  $m$  in the nanotubes of small diameters and with thin walls cannot support optical modes with high cavity quality ( $Q$ ) factor in the range of exciton transitions. The cavity  $Q$ -factor can be defined as  $E/\Delta E$ , where  $E$  is the energy and  $\Delta E$  is the half-width of the resonant narrow lines modulating the emission spectra.

Strong direct exciton resonances, together with the presence of optical modes with the high  $Q$ -factor, are prerequisites for the realization of light-matter coupling leading to the formation of exciton-polaritons in individual MoS<sub>2</sub> nanotubes.<sup>[43]</sup> It was also assumed that some features of polaritons can be observed in optical spectra measured in nanotube ensembles.<sup>[44]</sup> Theoretically, it was shown that only about 40% of the mode electric field intensity is concentrated inside the tube wall. In this case, the Rabi splitting can reach 400 meV in the high-quality tubular MoS<sub>2</sub> resonators.<sup>[43]</sup> This splitting exceeds the typical values for the resonators based on

classical semiconductors, such as GaAs or GaN. In real MoS<sub>2</sub> tubes supporting the WGMs, the noticeable inhomogeneous broadening prevents the realization of the strong coupling regime.

The weak coupling regime, when it realized, initiates the separation of optical modes into the upper (UP) and lower (LP) polariton branches, as well as broadening of the PL line with an increase in the detection angle relative to the normal to the tube (see Figure 3d,e). In our experiments with a high-aperture microobjective (detection angle ~25 degrees), the PL line is broadened.<sup>[43]</sup> There are no modes that could correspond to UPs, but they may be suppressed by strong absorption above exciton resonances. Nevertheless, we are currently refraining from making statements about observing polaritons in our individual MoS<sub>2</sub> tubes. This requires additional experiments with the rotation of a single tube at different angles, as well as selection of samples of highest quality. We believe that rapid progress in fundamental research and practical application of MoS<sub>2</sub> nanotubes is possible with thorough control of their structural and optical properties.

### 3.3 MoS<sub>2</sub> Nanotube and Nanoribbon Field-Effect Transistors

MoS<sub>2</sub> nanotube (NT) and nanoribbons (NR) compared to the MoS<sub>2</sub> flakes have the benefit of not having edges and edge states, and as a result have the potential for ideal subthreshold swing in field-effect transistors (FET). In the first report on the fabrication of FET based on MoS<sub>2</sub> nanotubes and nanoribbons grown by chemical vapour transport,<sup>[45]</sup> the tubes and ribbons were placed onto a Si wafer covered with 26 nm Al<sub>2</sub>O<sub>3</sub> prepared by atomic layer deposition (Figure 4). Top metallic contacts were formed using electron beam lithography followed by deposition of Sc/Ni (40 nm/20 nm). Back gate metal was deposited on the back of the Si wafer by electron-beam evaporation of Ti/Au (5 nm/100 nm). All transistors of such design have shown n-type channel conduction with ON/OFF current ratio of more than 10<sup>3</sup>, which far exceeded the prior value of 60 measured on much more defected MoS<sub>2</sub> nanotubes prepared by sulfurization of Mo–S–I nanowires.<sup>[46]</sup> The diameter of the tube was 55 nm, and the width of the nanoribbon was 321 nm. The extracted currents per width at drain-source voltage ( $V_{DS}$ ) of 0.3 V and back gate voltage ( $V_{BG}$ ) of 1 V was 1.02  $\mu\text{A}/\mu\text{m}$  and 0.79  $\mu\text{A}/\mu\text{m}$ , respectively. From a fit to the experimental data, a nominal charge density of  $1.10^{16} \text{ cm}^{-3}$  for the nanotube and ribbon, a mobility of 43.5  $\text{cm}^2/\text{Vs}$  and 36  $\text{cm}^2/\text{Vs}$ , respectively, and flat band voltage of  $-0.9 \text{ V}$  and  $-1 \text{ V}$  were obtained. The contact resistance of Sc contacts on MoS<sub>2</sub> nanotube was 39.6 k $\Omega$  at zero  $V_{BG}$ . The minimum sub-threshold swing for the ribbon was 200 mV/decade, which was much improved with respect to previous result of 10 V/decade.<sup>[47]</sup> Previous report was obtained on ribbons prepared by reactive ion etching of MoS<sub>2</sub> exfoliated flake, which possessed relatively rough edges with dangling bonds.

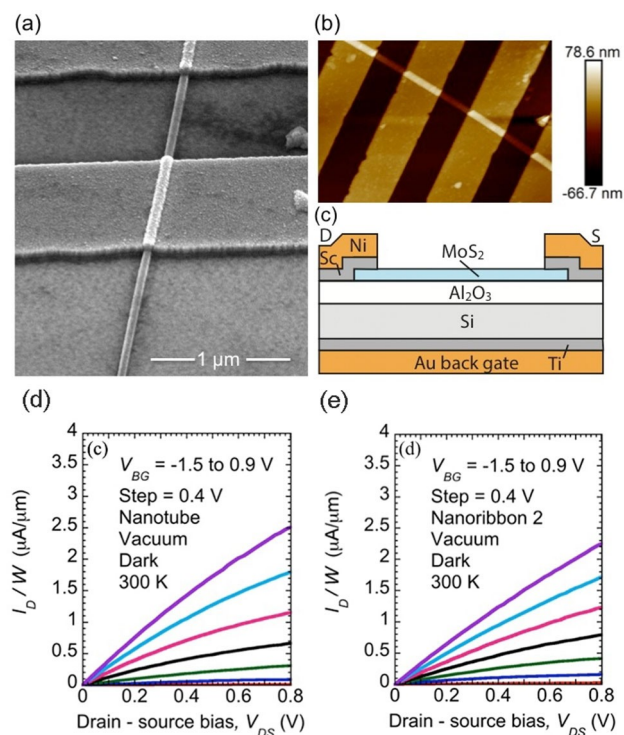


**Figure 4.** MoS<sub>2</sub> FETs (adopted from Ref. 46): (a) SEM image of a top-contacted MoS<sub>2</sub> nanotube; (b) the corresponding AFM image; (c) schematic cross-section of the device. d) Common source characteristics for the MoS<sub>2</sub> nanotube FET measured in vacuum. e) Common source characteristics for the MoS<sub>2</sub> nanoribbon FET measured in vacuum.

Before using such curved MoS<sub>2</sub> structures in nanoelectronics, many open questions need to be resolved, including how to form low-resistance contacts, how to form p-n junctions in them, and how to grow structures in predictable shape and at precise locations.

### 3.4 Field Emission from MoS<sub>2</sub> Nanotubes

Due to the high aspect ratio of length to diameter and their small dimensions, metallic and semiconducting nanowires are very interesting for applications in miniaturized field emission electron sources. In recent years, the focus of scientific investigations has been predominantly on carbon-based structures. However, carbon impurities are not desired in vacuum chambers, especially not in the semiconductor industry, so the MoS<sub>2</sub> materials represent a promising and interesting alternative. In order to investigate the field emission properties of nanotubes, they can be mounted on several micrometres' high silicon columns, which can be pre-prepared on highly conductive n-Si substrates.<sup>[15]</sup> Such a geometry ensured that the measured field emission was actually from the nanowire located there and not from other objects located on the substrate surface, e.g. scratches or particles. The silicon

column was flattened at the highest point, so that no significant field emission occurred there even at voltages of 1000 V or higher, and only after the nanotubes were mounted, a measurable field emission current was recorded. This arrangement was used to study the field emission properties of the MoS<sub>2</sub> structures.<sup>[15]</sup> Two directions of the tubes with regards to electric field were tested, parallel with emission from end of the nanotube, and perpendicular with emission from the lateral surface of another nanotube (Figure 5).<sup>[15]</sup> The samples were prepared inside the FEI Helios Nanolab 650 FIB SEM system. Electric contacts were made by Pt deposition. Diameter of the nanotubes used for these experiments was about 110 nm for vertically positioned tube and around 90 nm for lateral one.

Field emission (FE) measurements were performed in a diode configuration with a 10 MΩ resistor in series to the electrometer (protection against discharges) with a voltage source (Keithley 6517) in a vacuum chamber at pressures of about 10<sup>-9</sup> mbar. A metallized fine-meshed grid with Si support acted as an anode was separated from the cathode by a mica spacer of 50 μm thickness.<sup>[48]</sup> A voltage sweep with a slew rate of 1 V/s from 0 V up to 1000 V and then again down to zero V was conducted in order to characterize the I–V

characteristics of both samples. At maximum applied voltage of 1000 V (20 MV/m), field emission currents  $I_{\max}$  of 1.0 μA for the upright mounted nanotube and 11 μA for the lateral one were observed. The onset voltage for emission current of 1 nA was about 550 V for both orientations of the nanotubes. For voltages higher than 600 V (upright) and 700 V (lateral), a deviation from the ideal Fowler-Nordheim (FN) behaviour was noticed. This deviation is explained by Schottky barrier due to non-optimal transport mechanism between the nanotube and Si pillar, which is connected via sidewalls, in contrast to the lateral nanotube, which is connected by the both ends of the nanotube. A work function  $\Phi = 4.5$  eV was assumed for the upright nanotube<sup>[49,50]</sup> and a slightly higher value of 5.2 eV for the lateral one due to the varying emission areas from different crystallographic planes. The emission area estimated from the FN plots for the lateral tube was around 50 times larger than in the case of an upright tube, while field enhancement factors were found to be similar, i.e. 400 in case of the upright tube and 415 for the lateral one. The results were in good agreement with electrostatic finite element method simulations using COMSOL.<sup>[15]</sup> As expected from the geometry, a much larger value  $S$  for the emission area is obtained for the lateral nanowire ( $S = 5.5 \cdot 10^{-12}$  cm<sup>2</sup>) compared

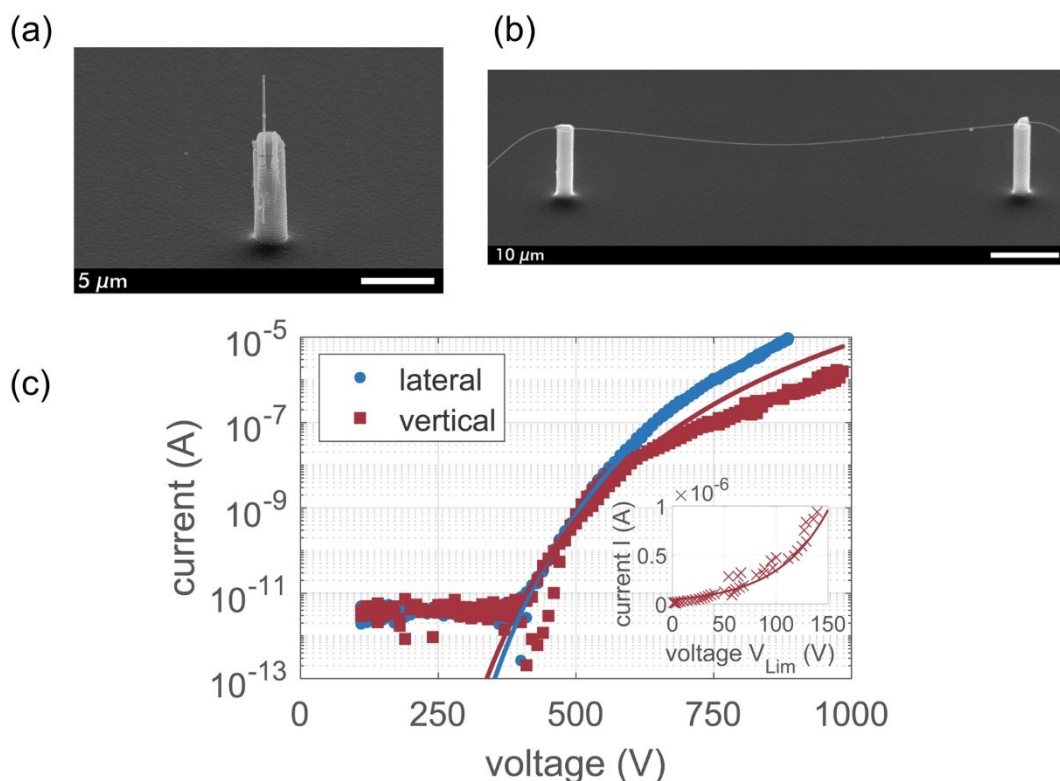


**Figure 5.** (adopted from Ref. 15): MoS<sub>2</sub> nanotubes with diameter around 100 nm mounted on As-doped n-Si columns: (a) vertical orientation with regard to the substrate; (b) parallel orientation; (c) current-voltage characteristics of the field emission from the vertical (red squares) and lateral (blue circles) MoS<sub>2</sub> nanotubes and regression curves using the FN-model for field emission of electrons (solid lines). The regression curve for the lateral nanotube (blue solid line) perfectly fits the measurement data, whereas in the vertical arrangement, a strong deviation occurs at higher voltages (red solid line). In the inset the extracted characteristics for a current limiting circuit for the vertical MoS<sub>2</sub> nanotube emitter is depicted.

to the vertical nanowire ( $S = 10 \cdot 10^{-14} \text{ cm}^2$ ). However, due to the surface texture, emission is not expected to be uniform over the entire surface, but rather from individual sharp-edged structures located at the end (vertical nanowire) or on the surface (lateral nanowire).

Finally, both samples were operated constantly at a voltage of 1000 V for one hour and the value of the emission current over time was measured in each case. The upper and lower 5% of the measured values were neglected for the calculation of the mean emission current  $I_{\text{mean}}$  and the relative deviation. For the vertical nanotube, a value of  $0.6 \mu\text{A} \pm 46\%$  was found for the  $I_{\text{mean}}$ . The lateral MoS<sub>2</sub> nanotube shows a comparable deviation value of about  $\pm 29\%$ , however, for a approx. 10 times higher  $I_{\text{mean}}$  of  $5.1 \mu\text{A}$ . The actual current fluctuations with constant voltage are too high for most practical applications. In previous works we presented circuits, which lead to a stabilization of the emission current ( $< 0.01\%$ ) by an n-channel MOSFET<sup>[51]</sup> or by a high voltage power amplifier driven by a proportional-integral controller.<sup>[52]</sup> This method of stabilizing the emission current may also be used for these types of emitters. For the vertical MoS<sub>2</sub> nanotubes, a negative current drift in the range of tens of nA/h was noticeable which indicates a continuous degradation of the vertical emitters with time. While the emission current of the vertical emitter decreased with time, an increase in the emission current for the lateral emitter with a value of  $\Delta I_{\text{drift}}$  of about  $2 \mu\text{A/h}$  was observed. Although individual emission centres on the lateral nanowire surface may degrade with time, the emission from the lateral surface as a whole actually effectively increases with increasing operating time. Thus, despite the emission current being about an order of magnitude higher at the same voltage, the lateral emitter exhibits less degradation compared to the vertical emitter. Since the lifetime of the emitter plays a very important role for practical applications, the lateral geometry seems to be superior to the vertical arrangement.

#### 4. Future Perspectives

Curved MoS<sub>2</sub> structures prepared at high temperatures in a long process for several weeks, which runs nearly at chemical equilibrium, are distinguished by low density of structural defects and a high aspect ratio. While a variety of allotropes were observed and structurally described, only a few of them were already investigated in details with regard to their physical properties. As an example, MoS<sub>2</sub> ribbons were studied only with respect to their vibration and gate controlled transport properties. The interface between both collapsed walls represents a unique 2D mirror plane composed of mutually rotated crystal blocks and sided by semi-spherical part-tubes at their edges. Such a structure guarantees a high anisotropy in transport properties. Theoretical descriptions of the energy level structure of MoS<sub>2</sub> microtubes, which spontaneously crystallize in metastable rhombohedral (3R) stacking<sup>[21]</sup> are still missing. Another unexplored field are MoS<sub>2</sub> tubular structures with chiral growth, which due to

transport anisotropy could under current induction form a magnetic field in this otherwise diamagnetic compound. The strong confinement of a MoS<sub>2</sub> nanotube as a quantum dot brings the regime of single-level quantum transport at low temperatures within reach. Strong spin-orbit interaction and spin splitting in the conduction band may lead to novel electronic shell structures, e.g., displaying threefold degeneracy and a spinless triple quantum Kondo effect SU(3).<sup>[53]</sup> Furthermore, the topological properties in particular in interaction with superconductivity are of high interest. Besides pure MoS<sub>2</sub> structures, noble-metals alloyed MoS<sub>2</sub> tubes also exist. It was reported that Au and Ag suppress chirality of the tubes and cause simultaneous growth of zigzag and arm-chair structures inside a single nanotube.<sup>[54]</sup> Physical properties of such alloyed or doped MoS<sub>2</sub> curved structures wait to be explored. The full potential of optical resonators based on MoS<sub>2</sub> micro- and nanotubes has not yet been revealed, although they possess such unique properties as subwavelength dimension, light polarization, superior optical confinement in the tube walls, and the possibility of polariton formation. Research in this direction may open up the possibility of using these MoS<sub>2</sub> tubes for nanophotonics, for creating lasers and polarization-sensitive sensors. The same applies to the prospects for using MoS<sub>2</sub> tubular structures in nanoelectronics as miniature transistors and field emitters.

#### Acknowledgements

M.R. thanks Prof. Francis Lévy, EPFL, for collaboration in pioneering research of MoS<sub>2</sub> tubular structures, and Research Agency of Republic Slovenia for funding. T.V.S. thanks the Russian Science Foundation (project #19-12-00273) for supporting the research of excitons and optical modes in nanotubes. A.K.H. acknowledges funding by the Deutsche Forschungsgemeinschaft, grants Hu1808/4-1 and Hu1808/6-1.

#### References

- [1] A. Enyashin, S. Gemming, G. Seifert, *Eur. Phys. J. Special Topics* **2007**, *149*, 103–125.
- [2] M. Remskar: *Comprehensive Nanoscience and Technology*. Volume 1. Nanomaterials, Andrews D.L., Scholes G.D., Wiederrecht G. P. (eds.), 315–330, London: Elsevier 2011.
- [3] U. Krishnan, M. Kaur, K. Singh, M. Kumar, A. Kumar, *Superlattices Microstruct.* **2019**, *128*, 274–297.
- [4] H. S. Nalwa, *RSC Adv.* **2020**, *10*, 30529–30602.
- [5] *Gmelin Handbook of Inorganic and Organometallic Chemistry* (Springer-Verlag, Berlin, 1995), 8th ed., Vol. B7.
- [6] J. Shi, et al., *Adv. Mater.* **2017**, *29*, 1701486 (1–9).
- [7] R. Akashi, et al., arXiv:1502.07480 [cond-mat.mtrl-sci].
- [8] F. Wypych, R. Schöllhorn, *J. Chem. Soc. Chem. Commun.* **1992**, *19*, 1386–1388.
- [9] K. F. Mak, et al., *Phys. Rev. Lett.* **2010**, *105*, 136805.
- [10] R. Coehoorn, C. Haas, R. A. De Groot, *Phys. Rev. B* **1987**, *35*, 6203.

- [11] M. Remskar, Z. Skraba, F. Cleton, R. Sanjines, F. Levy, *Appl. Phys. Lett.* **1996**, *69*, 351–353.
- [12] S. Reinhard, L. Pirker, C. Bäuml, M. Remskar, A. K. Hüttel, arXiv: 1904.05972.pdf, *Phys. Stat. Solidi, RRL* **2019**, *13*, 1900251.
- [13] D. R. Kazanov, et al., *Appl. Phys. Lett.* **2018**, *113*, 101106–1–101106–5.
- [14] S. Fathipour, et al., *Appl. Phys. Lett.* **2015**, *106*, 022114 –1–022114–4.
- [15] R. Łavrowski, et al., *J. Vac. Sci. Technol. B* **2020**, *38*, 032801–1–032801–11.
- [16] L. Margulis, G. Salitra, R. Tenne, M. Talianker, *Nature* **1993**, *365*, 113–114.
- [17] Y. Feldman, E. Wasserman, D. J. Srolovitz, R. Tenne, *Science* **1995**, *267*, 222–225.
- [18] M. Remskar, Dekker encyclopedia of nanoscience and nanotechnology V, **2004**, SCHWARZ, James A. (ur.). New York; Basel: M. Dekker, 1457–1465.
- [19] M. Remskar, Z. Skraba, F. Cleton, R. Sanjines, F. Levy, *Surf. Rev. Lett.* **1998**, *5*, 423–426.
- [20] M. Remskar, Z. Skraba, C. Ballif, R. Sanjines, F. Levy, *Surf. Sci.* **1999**, *433–435*, 637–641.
- [21] E. A. Laird, et al., *Rev. Mod. Phys.* **2015**, *87*, 703–764.
- [22] K. J. G. Götz, et al., *Phys. Rev. Lett.* **2018**, *120*, 246802–6.
- [23] M. Marganska, et al., *Phys. Rev. Lett.* **2019**, *122*, 086802–6.
- [24] Y. Li, N. Mason, *arXiv preprint* **2013**, arXiv:1312.3939.
- [25] K. Lee, G. Kulkarni, Z. Zhong, *Nanoscale* **2016**, *8*, 7755–7760.
- [26] R. Pisoni, et al., *Appl. Phys. Lett.* **2018**, *112*, 123101–3.
- [27] G. Seifert, et al., *Phys. Rev. Lett.* **2000**, *85*, 146–149.
- [28] K. F. Mak et al., *Phys. Rev. Lett.* **2010**, *105*, 136805–4.
- [29] I. Milosevic et al., *Phys. Rev. B* **2007**, *76*, 233414–4.
- [30] J. T. Ye et al., *Science* **2012**, *338*, 1193–1196.
- [31] D. Costanzo et al., *Nature Nanotechn.* **2016**, *11*, 339–344.
- [32] E. Piatti et al., *Nano Lett.* **2018**, *18*, 4821–31.
- [33] K. S. Novoselov, A. H. Castro Neto *Phys. Scr.* **2012**, 014006–6.
- [34] A. K. Hüttel, et al., *Phys. Rev. Lett.* **2009**, *102*, 225501–4.
- [35] C. Gong et al., *Nano Lett.* **2014**, *14*, 1714–1720.
- [36] S. Das et al., *Nano Lett.* **2013**, *13*, 100–5.
- [37] R. J. Wu et al. *Phys. Rev. Mater.* **2019**, *3*, 111001(R)–6.
- [38] P.-C. Shen et al., *Nature* **2021**, *593*, 211–217.
- [39] T. V. Shubina, et al., *Ann. Phys.* **2019**, *531*, 1800415–14.
- [40] O. O. Smirnova, I. A. Eliseyev, A. V. Rodina, T. V. Shubina, *J. Phys. Conf. Ser.* **2020**, *1482*, 012038–6.
- [41] I. A. Eliseyev, et al., *Phys. Status Solidi RRL* **2021**, 2100263–14, DOI: 10.1002/pssr.202100263.
- [42] D. Kazanov, M. Rakhlin, A. Poshakinskiy, T. Shubina, *Nano-materials* **2020**, *10*, 373–9.
- [43] J. Wang, T. Zhan, G. Huang, P. K. Chu, Y. Mei, *Laser Photonics Rev.* **2014**, *8*, 521–547.
- [44] S. S. Sinha, et al., *J. Phys. Chem. C* **2021**, *125*, 6324–6340.
- [45] S. Fathipour, et al., *Appl. Phys. Lett.* **2015**, *106*, 022114–4.
- [46] M. Strojnik, et al., *AIP Adv.* **2014**, *4*, 097114–5.
- [47] H. Liu, J. Gu, P. Ye, *IEEE Electron Device Lett.* **2012**, *33*, 1273–1275.
- [48] C. Prommesberger, C. Langer, R. Ławrowski, R. Schreiner, *J. Vac. Sci. Technol. B* **2016**, *35*, 012201.
- [49] S. Y. Lee, et al., *ACS Nano* **2016**, *10*, 6100–6107.
- [50] L. Britnell, et al., *Science* **2013**, *340*, 1311–1314.
- [51] S. Edler, et al., *J. Appl. Phys.* **2017**, *122*, 124503–6.
- [52] C. Langer, et al., *J. Vac. Sci. Technol. B* **2020**, *38*, 013202.
- [53] R. Lopez et al., *Phys. Rev. B* **2013**, *87*, 035135–12.
- [54] M. Remskar, Z. Skraba, P. Stadelmann, F. Levy, *Adv. Mater.* **2000**, *12*, 814–818.

Manuscript received: September 3, 2021  
Revised manuscript received: October 22, 2021  
Version of record online: November 26, 2021